Targetome

ORIGINAL ARTICLE

Open Access

https://doi.org/10.48130/targetome-0026-0060

Targetome **2026**, 2(6): e064

Genetic and pharmacological targeting of SNAI1 attenuates liver fibrosis in mice

Chuyue Pan[1#], Xu-zhe Zhang[1#], Xiao-wen Xu[1#], Zhao-lan Zeng[1], Stephen J. Weiss[2], Jie Liu[3*], Rong Fu[1*] and Zhao-Qiu Wu[1*]

[1] *State Key Laboratory of Natural Medicines, School of Pharmacy, China Pharmaceutical University, Nanjing 211198, China*
[2] *The Life Sciences Institute, Department of Internal Medicine, University of Michigan Medical School, Ann Arbor 48109, USA*
[3] *State Key Laboratory of Natural Medicines, School of Science, China Pharmaceutical University, Nanjing 211198, China*
[#] Authors contributed equally: Chuyue Pan, Xu-zhe Zhang, Xiao-wen Xu
* Correspondence: cpu-jill@163.com (Liu J); furong@cpu.edu.cn (Fu R); zqwu@cpu.edu.cn (Wu ZQ)

Abstract

Liver fibrosis, induced by viral hepatitis, alcohol abuse, and metabolic dysfunction-associated steatohepatitis (MASH), poses a severe threat to human health worldwide. As liver fibrosis is a critical and potentially reversible stage during liver disease progression, effective therapeutic options for liver fibrosis remain limited. In this study, we identified SNAI1, a multifunctional transcription factor, as a key promoter of liver fibrosis development. By analyzing single-cell RNA sequencing (scRNA-seq), β-galactosidase co-staining with cell-type-specific markers, and SNAI1 expression determined in isolated primary hepatic cells, we demonstrated that SNAI1 is predominantly expressed in hepatic stellate cells (HSCs) and is significantly elevated in fibrotic livers. HSC-specific deletion of *Snai1* resulted in markedly improved fibrosis-associated phenotypes induced by CCl_4, as evidenced by reduced levels of alanine aminotransferase (ALT) and aspartate aminotransferase (AST), decreased HSC activation, and collagen deposition in liver tissues. We further found that SNAI1 bound to the promoters of *ACTA2* and *COL1A1*, thereby regulating epigenetic histone acetylation at H3K4, H3K14, and H3K18, which subsequently enhanced HSC activation. Notably, pharmacological inhibition of SNAI1 using the lead compound LFW273 effectively prevented liver fibrosis progression in both CCl_4- and methionine-choline-deficient (MCD) diet-induced fibrotic mouse models, with efficacy comparable to the positive control drug, resmetirom. Collectively, our findings reveal a critical regulatory role of SNAI1 in liver fibrosis and establish SNAI1 as a promising drug target for anti-fibrotic therapy.

Keywords: Liver fibrosis; SNAI1; Hepatic stellate cell; LFW273; Lead compound

Citation: Pan C, Zhang XZ, Xu XW, Zeng ZL, Weiss SJ, et al. 2026. Genetic and pharmacological targeting of SNAI1 attenuates liver fibrosis in mice. *Targetome* 2(6): e064 https://doi.org/10.48130/targetome-0026-0060

Introduction

Liver fibrosis is a pathological consequence of chronic liver injury and inflammation, usually caused by viral hepatitis, alcohol-related liver disease (ALD), and metabolic dysfunction-associated steatohepatitis (MASH)[1,2]. However, liver fibrosis, as the final reversible stage before progression to liver cirrhosis and hepatocellular carcinoma (HCC), faces a great challenge in therapy[3,4]. The discovery of anti-fibrotic targets has advanced rapidly in recent decades, particularly for MASH-related fibrosis. Not only have semaglutide and resmetirom been approved by the US Food and Drug Administration (FDA), but other FGF21 analogues, such as efimosfermin alfa, are also currently under phase III clinical trials[5–8]. Admittedly, their effects on resolving fibrosis are moderate, and long-term effects require further evaluation. Elucidating the molecular mechanism of fibrosis progression and potential pharmacological therapeutic targets for liver fibrosis is thus urgently needed.

SNAI1 is one of the members of zinc-finger (ZF) transcription factors that function as a regulator of epithelial-to-mesenchymal transition (EMT) during embryonic development and tumor metastasis[9,10]. SNAI1 has been reported to promote the progression of renal fibrosis, dermal fibrosis, and pulmonary fibrosis by enhancing EMT[11–13]. However, lineage tracing has demonstrated that neither hepatocytes nor cholangiocytes undergo EMT in several murine models of hepatic fibrosis[14], which differs from other fibrotic diseases. It is hepatic stellate cells (HSCs) that are the most critical contributors during liver fibrosis; they reside in the space of Disse under physiological conditions and are activated to secrete extracellular matrix (ECM) after liver injury[1]. Thus, targeting HSC activation is a key strategy for the development of anti-fibrotic drugs. Previous studies on hepatic SNAI1 have primarily focused on hepatocytes[15,16], or have utilized it as one of the indicators of liver fibrosis[17,18]. Therefore, the systemic functions and downstream mechanisms of SNAI1 in HSCs, as well as its therapeutic potential as an anti-fibrotic drug target, remain to be investigated.

In this study, by integrating scRNA-seq, primary cell isolation, and *Snai1*-LacZ reporter mice, we demonstrated that SNAI1 is predominantly expressed in HSCs rather than in hepatocytes. HSC-specific *Snai1* knockdown showed decreased HSC activation and collagen production, thereby attenuating the progression of liver fibrosis. Mechanistically, we further identified that SNAI1 directly regulates the transcription of the two most representative fibrotic marker genes (*ACTA2* and *COL1A1*) by binding to their promoters. Finally, we evaluated the druggability of SNAI1 using a small-molecule inhibitor and validated its therapeutic efficacy in CCl_4-induced and MASH-associated fibrosis. Overall, these findings provide insights into the HSC-specific role and mechanism of SNAI1 in liver fibrosis, and suggest its potential as a viable anti-fibrotic drug target.

Methods and materials

Single-cell RNA sequencing analysis

The human *SNAI1* gene expression and location in various liver cell types were analyzed using public scRNA-seq data from the Gene

© The Author(s)

Expression Omnibus (GEO, www.ncbi.nlm.nih.gov/geo). The GSE256398 database includes data from three patients with metabolic dysfunction-associated steatotic liver disease (MASLD), four patients with MASH-associated fibrosis, four patients with MASH-associated cirrhosis, and six healthy controls[19]. Healthy individuals and non-fibrotic MASLD patients served as the Control group, and patients with MASH-associated fibrosis and cirrhosis were divided into the Fibrosis group. Raw scRNA-seq data were analyzed using the R package Seurat. Quality control retained cells with 200–6,000 detected genes, < 10% mitochondrial transcripts, and < 25,000 UMIs. Putative doublets were filtered out using scDblFinder. Data were log-normalized, and the top 2,000 highly variable genes were used for principal component analysis (PCA). Batch effects were integrated using Harmony across the first 15 principal components. Cells were clustered *via* the Louvain algorithm (resolution = 0.6), visualized using UMAP, and manually annotated into major liver lineages (HEP, ECS, EPS, HSCS, NK/T, B, DC) based on canonical marker genes. Differences in mean *SNAI1* expression between groups were evaluated using the two-sided Wilcoxon rank-sum test, with $P < 0.05$ considered statistically significant.

RNA sequencing analysis

Clinical datasets were acquired from GSE94417, GSE246221, and GSE267031. GSE94417 database included 109 individuals with non-fibrotic disease and 67 patients with hepatitis or cirrhosis[20]. Twenty-eight patients with MASLD and metabolic associated fatty liver disease (MAFLD)/MASH patients from databases GSE246221 and GSE267031, respectively, were also included in this study[21,22].

Mice

Mice were housed under standard specific-pathogen-free (SPF) conditions with free access to food and water; the temperature was maintained at 25 °C under a regular 12-h light/dark cycle. All animal procedures were approved by the institutional Animal Care and Use Committee of China Pharmaceutical University.

C57BL/6J wild-type mice (WT; male, 8–10-week-old) were purchased from Jiangsu Huachuang SinoPharmaTech Co., Ltd (Nanjing, China). *Snai1*-floxed (*Snai1*$^{flox/flox}$) mice and mice with *Snai1*-LacZ knock-in alleles have been described previously[9]. *Lrat*-Cre transgenic mice (T006205) were obtained from GemPharmatech (Nanjing, China) and crossed with *Snai1*$^{flox/flox}$ *mice* to generate *Snai1*$^{\Delta HSC}$ mice. All the primers for mouse genotyping were listed in Supplementary Table S1.

For CCl_4-induced liver fibrosis, age-matched mice (C57BL/6J, male, 8-week-old) were intraperitoneally injected with 10% CCl_4 (in olive oil; 10 mL·g^{-1}) or olive oil twice a week for 4 weeks. Bile duct ligation (BDL) surgery was performed as described before[23]. Briefly, mice were anesthetized and subjected to a 1 cm laparotomy, and the bile duct was exposed and ligated with 6–0 silk sutures. Two ligatures were placed in the proximal and distal portions of the bile duct, respectively, and then the bile duct was cut between the ligatures. The abdomen was closed in layers, and mice were taken care of to maintain body temperature until they were awake. Mice were sacrificed at the appropriate time to collect liver tissues. MCD diet (A02082002BR, research diets) was used to feed WT (C57BL/6J, male, 10-week-old) mice for 6 weeks to induce MASH-associated liver fibrosis. For pharmacological inhibition of SNAI1, LFW273 was intragastrically administered at the dose of 100 mg·kg^{-1}, and resmetirom was administered with 3 mg·kg^{-1} for oral administration.

Cell lines

HEK293 (SCSP-502), LX2 (SCSP-527), and RAW 264.7 (SCSP-5036) cells were obtained from the Cell Bank of the Chinese Academy of Sciences (Shanghai, China) and cultured in DMEM supplemented with 1% antibiotics and FBS (10% for HEK293 and RAW 264.7; 2% for LX2). All cells were cultured at 37 °C with 5% CO_2 supplied.

Primary hepatocytes, HSCs, Kupffer cells, and LSECs isolation

Primary hepatocytes and nonparenchymal cells (NPCs) were isolated as described in previous studies[23,24]. Primary HSCs, Kupffer cells (KCs), and liver sinusoidal endothelial cells (LSECs) were isolated from CCl_4-induced WT and *Snai1*$^{\Delta HSC}$ mouse livers. Briefly, anaesthetized mice were perfused with buffer SC-1 (137 mmol·L^{-1} NaCl, 5.4 mmol·L^{-1} KCl, 0.7 mmol·L^{-1} $NaH_2PO_4·H_2O$, 0.85 mmol·L^{-1} Na_2HPO_4, 10 mmol·L^{-1} HEPES, 2 mmol·L^{-1} $NaHCO_3$, 0.5 mmol·L^{-1} EGTA, 5 mmol·L^{-1} glucose), SC-2-I (SC-1 without EGTA but added 3.8 mmol·L^{-1} $CaCl_2·H_2O$) (containing Pronase E), and SC-2-II (containing collagenase D) for 5 min each. Digested liver was transferred into cold SC-2 buffer (without collagenase) and then gently suspended. The cell suspension was mixed with another digest buffer (SC-2 containing Pronase E, Collagenase D, and DNase I) for 20 min at 37 °C. The mixture was filtered through 70 μm cell strainers and centrifuged at 500 r·min^{-1} for 1 min. The precipitate was hepatocytes, and the supernatant contained NPCs. After centrifugation (2,200 r·min^{-1}, 8 min), NPCs were mixed with Nycodenz solution (10%) and were carefully layered onto the 15% Nycodenz solution for 30-min density gradient centrifugation. The first layer under clear buffer was HSCs, and the second layer was cells containing KCs and LSECs. The second layer was plated on a plastic dish for 20 min to collect KCs. CD146 beads (Miltenyi Biotec, 130–092–007) were used to obtain purified LSECs[25]. HSCs, KCs, and LSECs isolated from every three mice were combined into one sample for subsequent measurements.

Primary HSCs for RNA-seq were isolated from individual mice as described before[26]. Briefly, the liver was perfused with SC-1 for 2 min, followed by SC-2 with Pronase E for 5 min, and then SC-2 with Collagenase D for 7 min, at a flow rate of 5 mL·min^{-1}. The digested liver was suspended and transferred to 50 mL of SC-2 (containing Pronase E, Collagenase D, and 1% DNase I) for another 25 min digestion. The cells were filtered through 70 μm cell strainers and centrifuged at 580 × *g* for 10 min, and then resuspended in Nycodenz solution at a final concentration of 10%. Clear GBSS/B buffer was carefully layered onto the cell-Nycodenz mixture. Centrifugation was then performed at 1,380 × *g* for 17 min without braking, and HSCs were collected at the interface between GBSS/B and Nycodenz.

Histology

H&E and Sirius red staining of liver sections were performed as described previously[27]. Masson staining of liver sections was conducted based on the manufacturer's protocol (Servicebio, G1006). Frozen liver sections were used for Oil Red O staining[28].

β-gal staining

Frozen livers were sectioned and then treated with the Senescence *β*-Galactosidase Staining Kit (Beyotime, China). Briefly, after three PBS rinses and 15 min of fixation, liver sections were dipped in the working solution (Buffer A + B + C + X-Gal solution according to the instructions of the kit) at 37 °C overnight. The images were acquired by microscope (Olympus IX73, Japan) the next day[9].

Immunohistochemical staining

As described in our previous study[27,29], paraffin-embedded sections were deparaffinized and rehydrated by rinsing in xylene and ethyl alcohol. Antigen retrieval was performed using an antigen unmasking solution (Vector Laboratories), and 0.3% Triton X-100 was used for permeabilization. After being immersed in 1% H_2O_2 for 30 min, sections were blocked with 5% goat serum in 0.5% bovine serum albumin for another 30 min. Primary antibodies anti-α-SMA (Abcam, ab5694), anti-COL1A1 (Huabio, ET1609), anti-KI67 (Abcam, ab15580), and anti-p-H3 (Cell Signaling Technology, 9701s) were incubated overnight at 4 °C. The next day, the sections were incubated with biotin-labeled secondary antibody and ABC solution (Vector Laboratories) for 30 min, and then followed by DAB solution (Vector Laboratories) staining. The nuclei were marked by hematoxylin.

Immunofluorescent staining

LX2 cells were seeded on glass coverslips and treated with TGF-β (10 μmol·L^{-1}) and LFW273 (5 or 10 μmol·L^{-1}) for 48 h. Cells were then fixed with 4% paraformaldehyde and permeabilized with 0.1% Triton-X. After three PBS rinses and 30 min of blocking, primary antibody anti-COL1A1 (Huabio, ET1609, 1 : 200) and corresponding secondary antibody Alexa Fluor 488 (Invitrogen, A-11008) were used for staining. Images were acquired by a confocal laser scanning microscope (Carl Zeiss, LSM900). The quantification of COL1A1 in LX2 cells was calculated as integrated intensity/cell number.

Serum assay

Serum was collected for liver function tests by Wuhan Servicebio Technology Co., Ltd, including ALT, AST, total bile acid level (TBA), γ-glutamyl transpeptidase level (γ-GT), direct bilirubin level (DBIL), and total bilirubin level (TBIL).

Triglyceride (TG) and total cholesterol (TC) measurement

Serum and hepatic TG and TC levels were measured according to the manufacturer's protocol (Nanjing Jiancheng, A110-1-1, A111-1-1).

Real-time PCR

Real-time PCR was conducted as described in our previous studies[9,27]. The primer sequences are shown in Supplementary Table S2.

RNA sequencing

The RNA-sequencing experiments of primary HSCs and LX2 cells and their downstream data analyses were performed as previously described[27]. Original RNA-seq data were deposited in the GEO database with Accession No. GEO: GSE329196.

Immunoblotting

Total protein was extracted with RIPA lysis buffer (Thermo, 89901) and supplemented with protease and phosphatase inhibitor. Proteins were detected by their specific primary antibodies and visualized on film using HRP-conjugated secondary antibodies. Primary antibodies SNAI1 (Cell Signaling Technology, 3879S), SLUG (Abcam, ab51772), α-SMA (Abcam, ab5694), COL1A1 (Huabio, ET1609), β-actin (Santa Cruz Biotechnology, sc47778), and β-tubulin (Santa Cruz Biotechnology, sc5274) were used.

Chromatin immunoprecipitation (ChIP)

As described in previous studies[30], cells were fixed in 1% formaldehyde for 10 min and incubated in 1.25 mol·L^{-1} glycine for 5 min at room temperature. After washing with cold PBS twice, cells were lysed in IP lysis buffer (50 mmol·L^{-1} Tris-HCl, 150 mmol·L^{-1} NaCl, 1 mmol·L^{-1} EDTA, 1% NP-40, 0.05% SDS, pH 7.4), supplemented with protease inhibitor cocktail for 20 min on ice. The cell lysates were sonicated to obtain DNA fragments of approximately 200–1,000 bp in length. The supernatants were pre-cleared with protein A/G beads and treated with salmon sperm DNA to block nonspecific binding (Thermo Fisher, 15632011) at 4 °C for 1 h. For the sheared chromatin, 10% of the lysate was used as input control, and the rest was incubated overnight with the following antibodies against Flag (Sigma, F3165), acetyl-histone H3 (K4; Abcam, ab176799), acetyl-histone H3 (K18; Cell Signaling, 9675), acetyl-histone H3 (K14; Cell Signaling, 7627), tri-methyl-histone H3 (K27; Cell Signaling, 9377), or Rabbit IgG (Abcam, ab172730) with rotation at 4 °C, followed by an additional incubation using precleared protein A/G beads for 1 h at 4 °C. After standing for 10 min and centrifugation, the chromatins bound to the beads were subjected to sequential washes: once with low-salt wash buffer, once with high-salt wash buffer, and twice with TE buffer. Subsequently, elution was performed twice using elution buffer (1% SDS, 0.1 mol·L^{-1} $NaHCO_3$), and the DNA-protein complexes were then subjected to an overnight incubation at 65 °C with 0.2 mol·L^{-1} NaCl. After incubating with RNase A for another 30 min at 37 °C the next day, proteinase K (Thermo Fisher, AM2548) was subsequently added, and the mixture was incubated at 45 °C for 2 h. Purification of the bound DNA was performed with a kit (Sigma-Aldrich, NA1020) following the manufacturer's protocol, and was subsequently analyzed by PCR. Primers were designed to span the proximal, middle, and distal regions of the promoter (−2 kb to 0), and representative images are shown in corresponding figures. Primer sequences are provided in Supplementary Table S3.

Luciferase

The ~2.0 kb fragment of the human *COL1A1* promoter (−2,000–0) and the ~2.1 kb fragment of the human *ACTA2* promoter (−2000–0) were synthesized by GenScript and subcloned into the pGL3-basic luciferase reporter vector. Control or *SNAI1*-overexpressing LX2 cells were transfected with *COL1A1* or *ACTA2* reporter constructs and the pRL-TK Renilla luciferase control construct. Dual-luciferase reporter assays were performed according to the manufacturer's instructions (YEASEN, 11402-E).

BODIPY staining

Cells were fixed with 4% paraformaldehyde and stained by incubating cells with 0.5 mmol·L^{-1} BODIPY 493/503 (Life Technologies) for 30 min[31]. The images were acquired by a confocal laser scanning microscope (Carl Zeiss LSM900). The quantification of BODIPY staining was calculated as integrated intensity/cell number.

Statistical analysis

All data in this study are presented as mean ± SEM and were graphed using GraphPad PRISM 9. A two-tailed Student's t-test was used for statistical analysis of the two-group comparisons; ordinary one-way ANOVA with Dunnett's multiple comparisons test and one-way ANOVA with Newman–Keuls multiple comparisons test were used for the statistical analysis of differences between multiple groups. A P value < 0.05 was considered statistically significant.

Results

SNAI1 expression in HSCs correlates with the development of liver fibrosis

To explore the role of SNAI1 in liver fibrosis, we first examined its expression in healthy and fibrotic livers. Analysis of a public microarray dataset (GEO: GSE94417) revealed that fibrotic tissues exhibited higher *SNAI1* expression compared with non-fibrotic individuals (Fig. 1a). Additionally, we found that the expression of *SNAI1* was positively correlated with the expression of fibrosis-associated genes, including *ACTA2*, *COL1A1,* and *COL3A1* in patients with MAFLD or MASH (GEO: GSE246221 and GSE267031) (Fig. 1b; Supplementary Fig. S1a and S1b). In order to investigate which cell types express *SNAI1*, we subsequently analyzed single-cell transcriptomic data from livers of healthy individuals and patients with liver cirrhosis (GSE256398). These analyses showed that *SNAI1* was mainly expressed in HSCs and endothelial cells (ECs) (Fig. 1c); however, under fibrotic conditions, *SNAI1* expression was specifically upregulated in HSCs (Fig. 1d). Moreover, similar results were observed in mouse models. CCl_4 injection and BDL surgery were used to induce liver fibrosis in *Snai1*-LacZ mice, in which β-gal expression reflects the SNAI1 levels in liver tissues[9] (Fig. 1e and f; Supplementary Fig. S1c and S1d). SNAI1 expression was markedly increased in CCl_4-treated mice compared with mice injected with olive oil (Control) (Fig. 1e and f). Notably, the co-staining revealed that β-gal signals colocalized with HSC markers (α-SMA or COL1A1) but not with KC marker F4/80 or the LSEC marker CD31 (Fig. 1e and f; Supplementary Fig. S1c and S1d). Furthermore, we confirmed that SNAI1 was predominantly expressed in HSCs using real-time PCR and immunoblotting on isolated primary mouse liver cells (Fig. 1g and h; Supplementary Fig. S1e). Hepatocytes barely expressed SNAI1, whereas HSCs exhibited the highest expression level of SNAI1 among all liver cell types. Consistently, SNAI1 expression in HSCs was upregulated during fibrosis progression.

HSC-specific *Snai1* deletion attenuates the progression of liver fibrosis

To elucidate the functional relevance of SNAI1 in HSCs during liver fibrosis *in vivo*, we generated HSC-specific *Snai1*-deficient mice by crossing *Lrat*-Cre mice with *Snai1*-floxed mice (Fig. 2a; Supplementary Fig. S2a). As expected, the mRNA and protein levels of SNAI1 in primary HSCs isolated from mouse livers were significantly reduced in $Snai1^{\Delta HSC}$ mice compared with $Snai1^{flox/flox}$ mice (Fig. 2b). Having confirmed that *Snai1* deletion in HSCs did not affect the baseline liver histology and functions (Supplementary Fig. S2b and S2c), we proceeded to investigate whether *Snai1* deficiency in HSCs was able to protect against CCl_4-induced liver fibrosis (Fig. 2a). As shown in Fig. 2c, *Snai1* HSC-deficient mice had lower levels of ALT and AST relative to control mice after CCl_4 injection, suggesting attenuated liver injury. Moreover, $Snai1^{\Delta HSC}$ mice exhibited lower collagen deposition and reduced HSC activation, as assessed by Masson staining, Sirius red staining, and anti-α-SMA immunohistochemical staining or immunoblotting, respectively (Fig. 2d–f). Consistently, CCl_4-treated $Snai1^{\Delta HSC}$ mice showed significantly decreased expression of genes involved in HSC activation and collagen homeostasis, such as *Acta2*, *Col1a1*, *Col3a1*, *Col6a3*, *Timp1*, *Fap,* and *Mmp2* (Fig. 2g). In addition, the expressions of genes encoding pro-inflammatory cytokines and chemokines (*Tnf*, *Ccl5,* and *Ccl2*) were downregulated in $Snai1^{\Delta HSC}$ mouse livers (Fig. 2g), whereas expressions of *Col1a2*, *Timp2*, *Tgfb1-3*, *Il1b,* and *Il6* remained unchanged (Supplementary Fig. S2d). Given that promoting liver regeneration is a promising strategy for fibrosis treatment[32], we examined hepatocyte proliferation and observed a slight increase in $Snai1^{\Delta HSC}$ mice (Fig. 2h and i), supporting that HSC-specific *Snai1* deletion attenuates hepatic fibrosis in part by promoting liver regeneration.

Collectively, these findings demonstrated that the HSC-specific *Snai1*-deficiency protects against liver fibrosis by alleviating liver injury, HSC activation, collagen deposition, and liver inflammation.

SNAI1 modulates the activation of HSCs by directly promoting the transcription of *ACTA2* and *COL1A1*

Activation of HSCs is one of the critical molecular events driving liver fibrosis[33]. Considering that SNAI1 was specifically increased in fibrotic HSCs, we subsequently examined whether the expression of SNAI1 contributes to HSC activation. TGF-β treatment induced SNAI1 expression in LX2 cells (Fig. 3a), and a progressive increase in *Snai1* mRNA level was observed as primary HSCs transitioned from a quiescent to an activated state (Fig. 3b). Transcriptomic and RT-PCR analysis of activated primary HSCs isolated from $Snai1^{flox/flox}$ and $Snai1^{\Delta HSC}$ mice both revealed significant reductions in representative pro-fibrotic markers, *Acta2* and *Col1a1* (Fig. 3b and c). Consistently, other fibrosis-related genes, including *Fn1*, *Timp1*, *Col4a3*, *Col7a1*, *Col11a1*, and *Mmp8,* also decreased in primary HSCs from $Snai1^{\Delta HSC}$ mice, suggesting that *Snai1* deficiency led to the alleviation of HSC activation. In contrast, the quiescent HSC signatures *Lrat* and *Ecm1* showed no significant difference between the two groups of mice[34] (Fig. 3c). ECM structural constituent and ECM-receptor interaction signaling pathways were remarkably inhibited in *Snai1*-deleted primary HSCs (Fig. 3d; Supplementary Fig. S3a). Similar findings were obtained by the RNA-seq analysis of LX2 cells transfected with si*SNAI1* (Supplementary Fig. S3b and S3c). The regulatory relationship between SNAI1 and fibrotic markers (*ACTA2* and *COL1A1*) was further confirmed by *SNAI1* overexpression and silencing in LX2 cells. Overexpression of *SNAI1* elevated the mRNA and protein levels of α-SMA and COL1A1, whereas *SNAI1* knockdown abolished these effects (Fig. 3e and f; Supplementary Fig. S3d and S3e). SNAI1 is a well-known versatile transcription factor regulating various genes in many physiological and pathological processes, such as EMT (*E-cad*, *N-cad*), inflammation (*Ccl5* and *Cxcl10*), and ECM accumulation (*Mmp2*, *Mmp13*)[30,35,36]. We therefore generated luciferase reporter constructs containing the *ACTA2* or *COL1A1* promoter. In LX2 cells, *SNAI1* overexpression significantly increased the activity of both promoters under basal conditions and following TGF-β stimulation (Fig. 3g). Because SNAI1 binds E-box motifs within target-gene promoters to regulate transcription[9,10,30], we performed ChIP assays to assess its direct promoter occupancy. The ChIP assays confirmed SNAI1 binding to the *ACTA2* and *COL1A1* promoters (Fig. 3h). Moreover, SNAI1 increased histone H3 acetylation at K4, K14, and K18 at these promoters, while exerting no significant effect on histone methylation (Fig. 3i).

In summary, we demonstrated that SNAI1 modulates HSC activation and ECM biosynthesis by directly binding to the *ACTA2* and *COL1A1* promoters, enhancing the histone acetylation modification, increasing chromatin accessibility, and thereby leading to the transcription of *ACTA2* and *COL1A1*.

Pharmacological inhibition of SNAI1 attenuates HSC activation

Accumulating evidence has shown that genetic inhibition of *Snai1* has been shown to prevent HSC activation and liver fibrosis, indicating that SNAI1 might be a promising drug target for

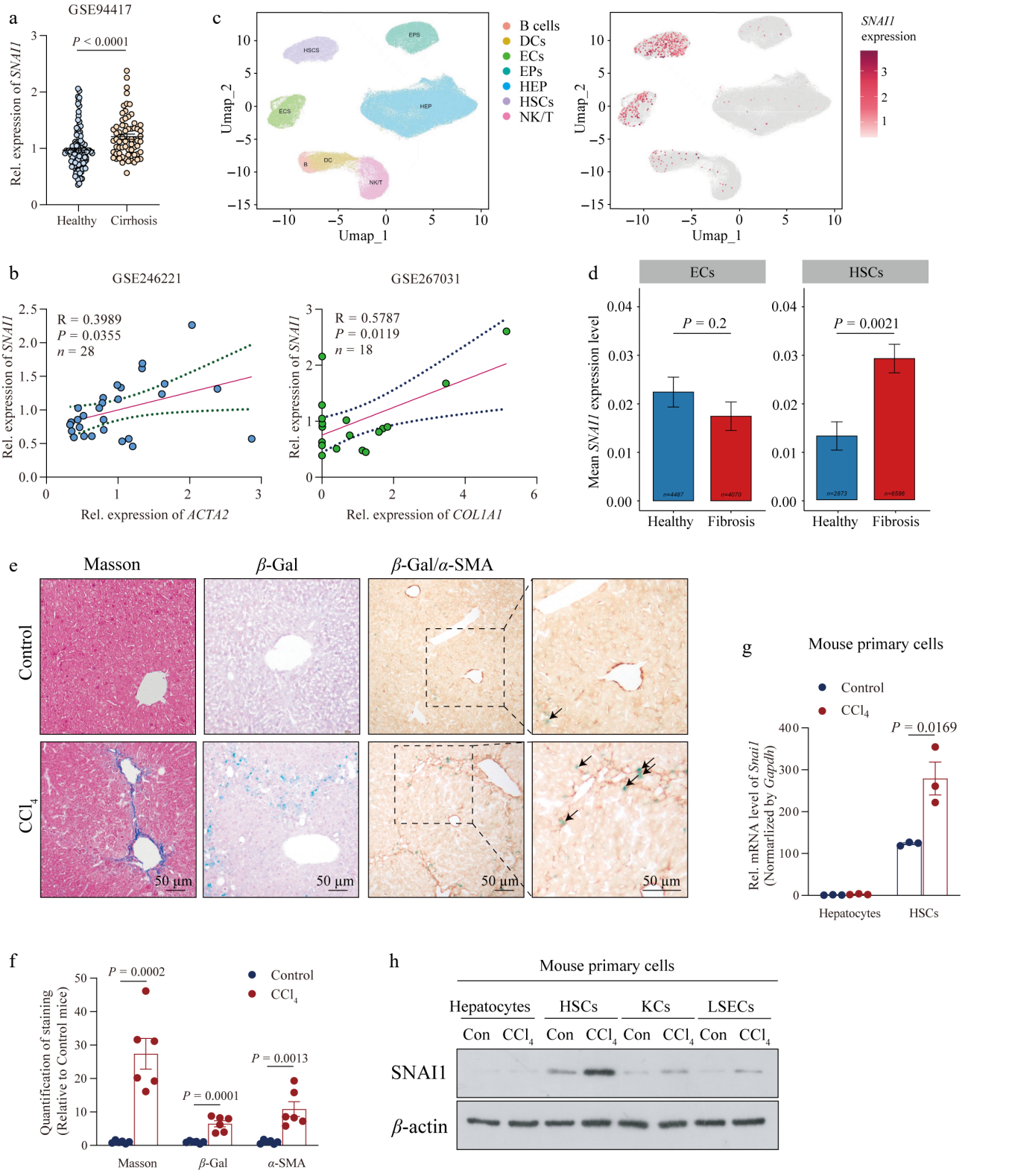


Fig. 1 SNAI1 expression in HSCs was upregulated during the progression of liver fibrosis. (a) Relative mRNA level of *SNAI1* acquired from the Gene Expression Omnibus (GSE94417) in livers from healthy controls or patients with cirrhosis. (b) Correlation of relative *SNAI1* expression with *ACTA2* and *COL1A1* in patients with MASH. Genetic data acquired from GSE246221 and GSE267031, respectively. (c) Single-cell transcriptome analysis of data from GSE256398; UMAP visualization of liver cell clusters based on human scRNA sequencing (left). Red dots represent the expression of *SNAI1* (right). (d) Mean *SNAI1* expression level in endothelial cells (ECs) and HSCs. (e) Representative images of Masson staining, β-gal staining, and β-gal/α-SMA co-staining in mice injected with oil (Control) and CCl_4. Arrows indicate the positive area of β-gal/α-SMA. Scale bar: 50 μm. (f) Quantification of the positive area in Fig. 1e. Primary hepatocytes, HSCs, KCs, and LSECs were isolated from liver tissues in mice subjected to oil or CCl_4 for 4 weeks. (g) mRNA levels of *Snai1* in hepatocytes and HSCs. (h) Protein levels of SNAI1 in hepatocytes, HSCs, KCs, and LSECs. Data are presented as mean ± SEM. $P < 0.05$ indicates a significant difference. All data were analyzed by two-tailed Student's t-test except data in (d) using Wilcoxon Mann–Whitney test.

https://doi.org/10.48130/targetome-0026-0060

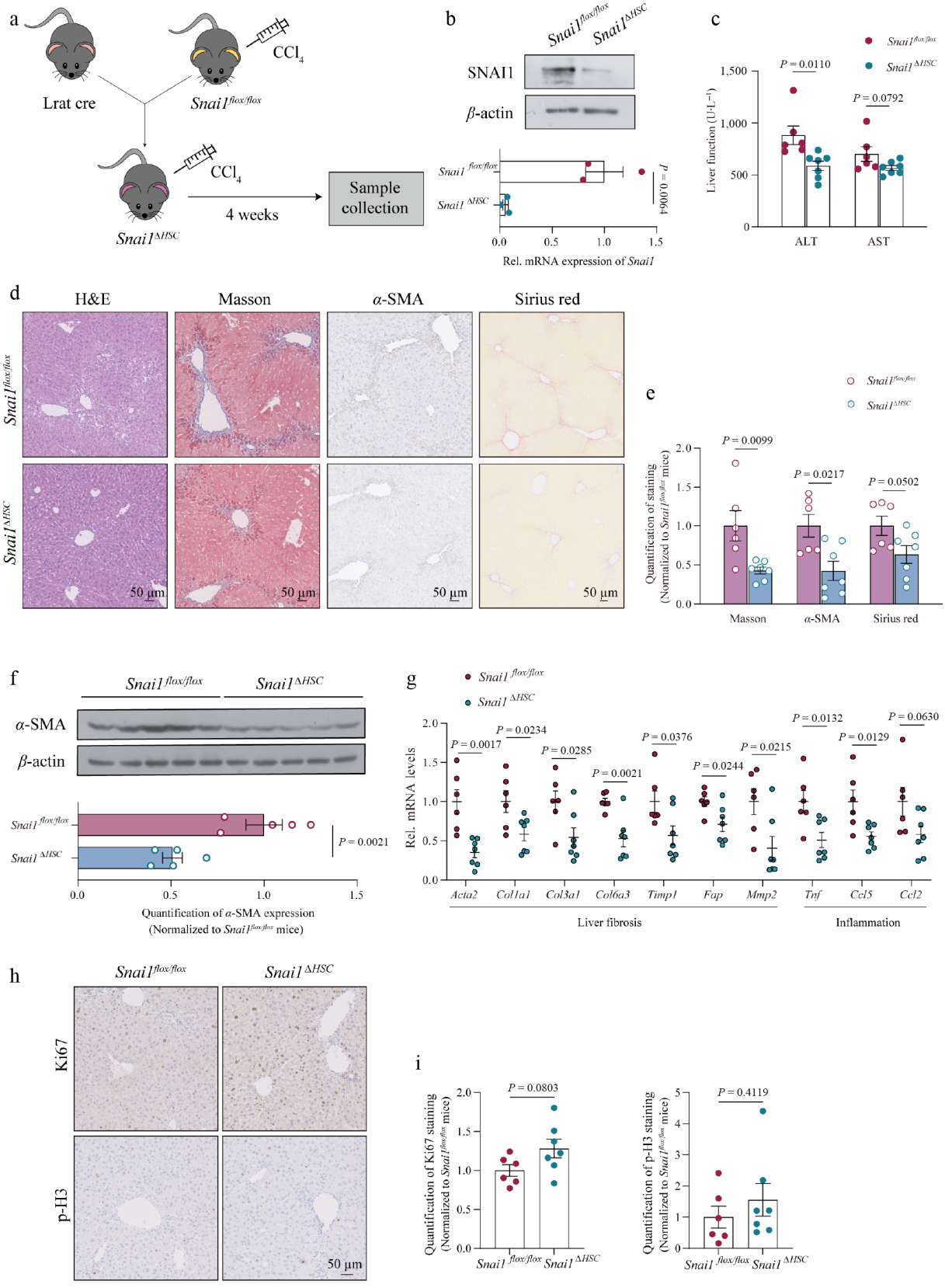


Fig. 2 HSC-specific deficiency of *Snai1* protected mice from CCl_4-induced liver fibrosis. (a) Schematic of the *Snai1*$^{\Delta HSC}$ mouse generation strategy and 4-week CCl_4-induced fibrotic mouse model. (b) SNAI1 protein and mRNA levels of primary HSCs were isolated from *Snai1*$^{flox/flox}$ and *Snai1*$^{\Delta HSC}$ mouse liver. *Snai1*$^{flox/flox}$ and *Snai1*$^{\Delta HSC}$ mice were injected with CCl_4 twice a week for 4 weeks ($n = 6$ for *Snai1*$^{flox/flox}$ mice and $n = 7$ for *Snai1*$^{\Delta HSC}$ mice). (c) Serum ALT and AST levels. (d) Representative images of H&E, Masson staining, α-SMA immunohistochemistry staining, and Sirius red staining. Scale bar: 50 μm. (e) Quantification of positive areas in (d). (f) Immunoblotting and quantification of α-SMA. (g) The mRNA levels of collagen-associated genes and pro-inflammatory genes. (h) Representative images and (i) positive signal quantification of Ki67 and p-H3 staining in liver sections. Scale bar: 50 μm. Data are presented as mean ± SEM. $P < 0.05$ indicates a significant difference. All data were analyzed by a two-tailed Student's t-test.

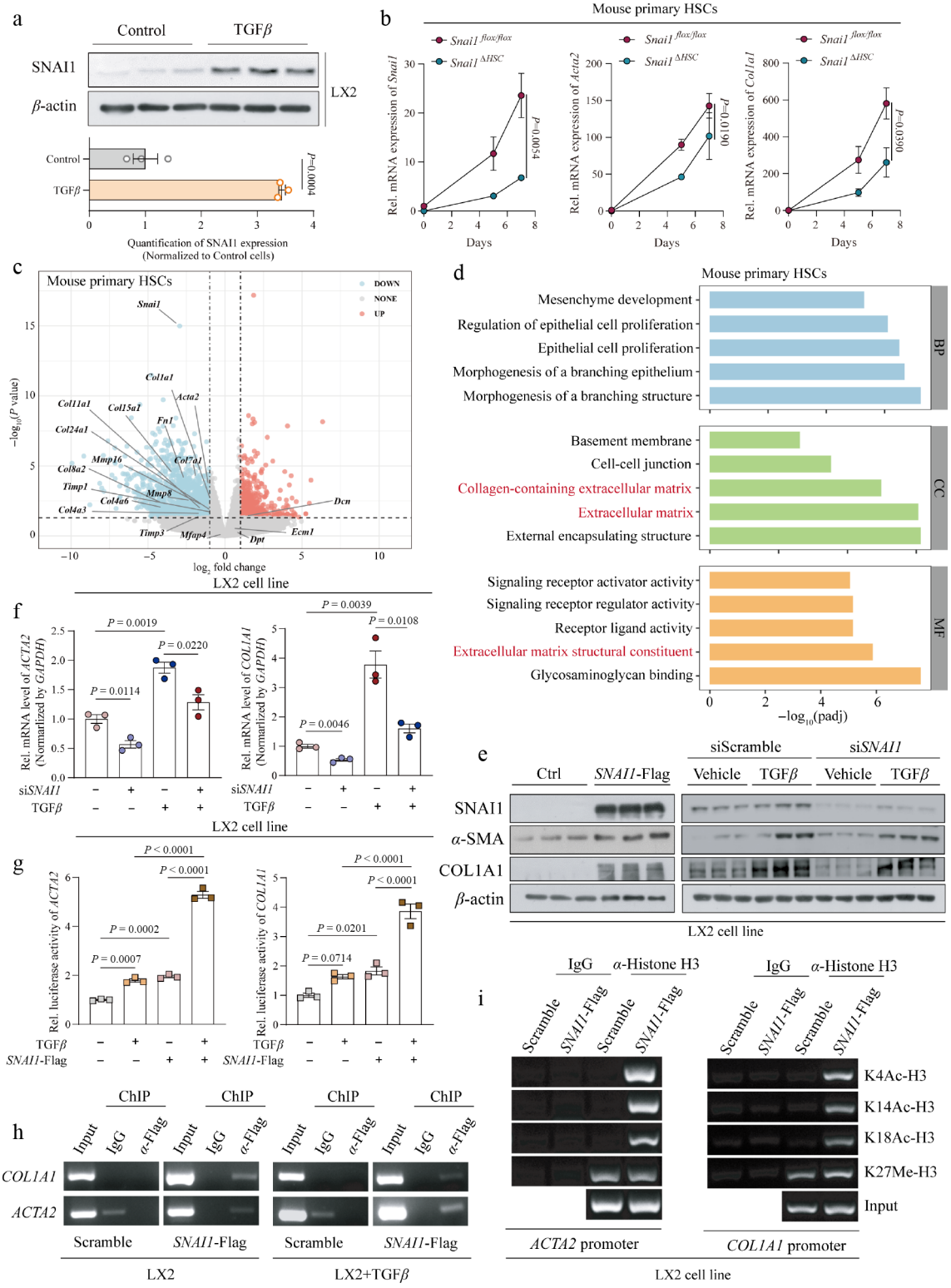


Fig. 3 *Snai1* enhanced the activation of HSCs. (a) Protein level of SNAI1 in LX2 cells treated with 10 μmol·L^{-1} TGF-*β* for 48 h. (b) mRNA levels of *Snai1*, *Acta2*, and *Col1a1* in primary HSCs from *Snai1*$^{flox/flox}$ and *Snai1*$^{\Delta HSC}$ mice cultured for 0, 5, and 7 d. The *P* value showed a significant difference by calculating the area under the curve (AUC). (c) Volcano plots of differentially expressed genes ($log_2FC > 1$ and *P* value < 0.05) between activated primary HSCs isolated from *Snai1*$^{flox/flox}$ and *Snai1*$^{\Delta HSC}$ mice. (d) Downregulated pathways analyzed by Gene Ontology (GO) pathway enrichment analysis. (e) The protein levels of SNAI1, *α*-SMA, and COL1A1 in LX2 cells transfected with an empty vector and *SNAI1*-Flag plasmid (left) or siScramble and si*SNAI1*, treated with or without TGF-*β* (right). (f) Gene expression of *Acta2* and *Col1a1* in LX2 cells. Cells were transfected with siRNA (siScramble and si*SNAI1*) and treated with 10 μmol·L^{-1} TGF-*β* for 48 h. (g) Transcriptional activity of *Acta2* and *Col1a1* in LX2 cells overexpressing *SNAI1* and treated with TGF-*β*. (h) Representative images of ChIP-PCR analysis confirming the loading of SNAI1 on the promoters of *ACTA2* and *COL1A1* in LX2 cells. (i) Representative images of ChIP-PCR analysis to determine the recruitment of H3K4Ac, H3K14Ac, and H3K18Ac to the *ACTA2* and *COL1A1* promoters in LX2 cells with *SNAI1* overexpressed. Data are presented as mean ± SEM. $P < 0.05$ indicates a significant difference. All data were analyzed by a two-tailed Student's t-test, and data in (g) were analyzed by one-way ANOVA with the Newman–Keuls multiple comparison test.

anti-fibrotic therapy. We have previously designed and synthesized a novel SNAI1 inhibitor named LFW273, which proved to improve atherosclerosis[30] (Fig. 4a). LFW273 enhanced the degradation of SNAI1 by accelerating its ubiquitination (Supplementary Fig. S4a and S4b). Since low concentrations of LFW273 (IC_{50} = 36.20 μmol·L^{-1}) had no effect on cell viability (Supplementary Fig. S4c), we used 5 or 10 μmol·L^{-1} LFW273 to treat LX2 cells and primary HSCs for subsequent investigation. As a result, LFW273 significantly reduced the protein level of SNAI1 while having no effect on its transcription (Fig. 4b and c; Supplementary Fig. S4d). TGF-β stimulation increased the expression of classical HSC activation markers α-SMA, type I collagen, and fibronectin 1 (*FN1*), all of which were dose-dependently suppressed after LFW273 treatment (Fig. 4b–d; Supplementary Fig. S4d and S4e). We also observed reduced transcriptional activity of *ACTA2* and *COL1A1* after 5 μmol·L^{-1} LFW273 treatment in LX2 cells, similar to that seen in *SNAI1* knockdown cells (Fig. 4e). Additionally, the inhibition of SNAI1 by LFW273 did not cause the compensatory increase but rather a slight reduction of SLUG, which belongs to the same family as SNAI1 (also called SNAI2) and was upregulated by TGF-β (Supplementary Fig. S4f). To further explore the pharmacological mechanism of LFW273 on HSC activation, we performed RNA-sequencing on LFW273- or vehicle-treated primary HSCs. The markedly decreased expression of fibrotic genes such as *Acta2*, *Col1a1*, *Tgfb2*, *Tgfb3*, *Col8a1*, *Col4a6*, *Mfap4*, and *Bmp10* suggested the inhibition of the TGF-β signaling pathway and HSC activation (Fig. 4f). Consistently, vascular smooth muscle contraction, ECM-receptor interaction, and TGF-beta signaling pathway were found decreased in KEGG enrichment analysis in LFW273-treated HSCs (Fig. 4g). In line with the transcriptional changes observed in *Snai1*-specific knockout HSCs (Supplementary Fig. S3a), KEGG analysis of LFW273-treated primary HSCs revealed upregulation of steroid biosynthesis and insulin resistance pathways (Fig. 4g). BODIPY staining further confirmed increased lipid droplet accumulation in LFW273-treated primary HSCs, a feature associated with a more quiescent-like state compared with cells treated with vehicle[33] (Fig. 4h). Moreover, ChIP assays revealed that SNAI1 binds to the promoter of *PPARG*, which was reported to be involved in HSC retinyl ester accumulation, and this binding was relieved in *SNAI1*-overexpressing cells[37,38] (Supplementary Fig. S4g). These findings are consistent with a published report and support that LFW273 promotes lipid accumulation in HSCs through reducing SNAI1 expression and thereby relieving SNAI1-mediated suppression of *PPARG* transcription. Of note, the suppression of *ACTA2* and *COL1A1* transcription was abolished in si*SNAI1*-transfected LX2 cells, suggesting that the efficacy of LFW273 depends on SNAI1 (Fig. 4i; Supplementary Fig. S4h). All the results confirmed that LFW273 treatment protects HSCs from activation, reduces collagen production, and promotes the quiescent state by reducing the transcriptional activation of *ACTA2* and *COL1A1*.

Pharmacological inhibition of SNAI1 alleviates liver fibrosis

After examining the function of LFW273 on HSC activation *in vitro*, we further aimed to evaluate the therapeutic potential of LFW273 in liver fibrosis. Mice were subjected to CCl_4 for 4 weeks to induce hepatic fibrosis (Fig. 5a). CCl_4 injection resulted in obvious liver injury and collagen deposition (Fig. 5b–d). Compared with fibrotic mice treated with vehicle, LFW273-treated mice showed significantly lower levels of ALT and AST, indicating reduced chemical-induced liver damage (Fig. 5b). Masson staining, Sirius red staining, and COL1A1 immunohistochemical staining showed reduced collagen accumulation following LFW273 administration. In parallel, α-SMA immunohistochemistry indicated reduced HSC activation after LFW273 treatment (Fig. 5c and d). The mRNA levels of fibrotic markers (*Acta2*, *Col1a1*, *Col1a2*, and *Timp1*) and inflammatory genes (*Il6* and *Ccl2*) were significantly decreased in LFW273-treated mice (Fig. 5e; Supplementary Fig. S5a). We further confirmed the protein levels of α-SMA and type I collagen in liver tissues using immunoblotting (Fig. 5f).

To investigate whether LFW273 could reverse pre-existing liver fibrosis, mice received CCl_4 injection for 3 weeks, followed by another 4-week LFW273 treatment together with CCl_4 injection (Fig. 6a). Hepatic SNAI1 was substantially reduced after LFW273 treatment (Fig. 6b). Compared with mice treated with vehicle, decreased serum ALT and AST, reduced collagen deposition, and lower α-SMA expression were observed in mice that received LFW273 treatment (Fig. 6c–e). mRNA levels of fibrosis-related genes such as *Acta2*, *Col1a1*, and *Tgfb2* were downregulated after LFW273 treatment (Fig. 6f). Moreover, liver inflammation was relieved in mice with LFW273 administration, as reflected by decreased expression of genes encoding pro-inflammatory cytokines (*Tnf*, *Il6,* and *Il1b*) and chemokines (*Ccl2* and *Cxcl10*) (Fig. 6f). Overall, LFW273 was efficient in preventing and reversing CCl_4-induced liver fibrosis.

We further assessed the safety of LFW273 administration. Histological staining of major organs showed minimal toxic effects after the 4-week treatment (Supplementary Fig. S5b). The acute toxicity study revealed no significant differences between mice administered intragastrically with vehicle and 1 g·kg^{-1} LFW273 (Supplementary Fig. S5c).

Taken together, our findings demonstrated that the novel small-molecule compound LFW273, which functions as an inhibitor of SNAI1, prevents the development of CCl_4-induced liver fibrosis with a superior safety profile.

SNAI1 pharmacological inhibitor LFW273 ameliorates liver fibrosis accompanied by MASH

Considerable evidence has revealed that liver fibrosis can be caused by viral hepatitis, ALD, and MASH, and that MASH is becoming the most common liver disease worldwide; however, alleviating liver fibrosis in this context remains challenging[39]. Until now, only resmetirom and semaglutide have been approved by the FDA for MASH therapy and have been reported to attenuate fibrosis progression[5–7]. Therefore, developing novel, effective pharmacotherapies for MASH is urgently needed. Here, we evaluated the anti-fibrotic function of LFW273 and made a comparison with resmetirom in the MCD-induced MASH model with fibrosis. In this model, mice were fed an MCD diet for 2 weeks and then received LFW273 or resmetirom treatment for another 4 weeks, while neither drug affected body weight (Fig. 7a). MCD feeding resulted in significant increases in serum ALT, AST, TBA, γ-GT, DBIL, and TBIL, and both LFW273 and resmetirom treatment improved these liver function abnormalities (Fig. 7b; Supplementary Fig. S6a). H&E and Oil Red O staining showed that SNAI1 inhibition or resmetirom treatment reduced hepatic steatosis (Fig. 7c; Supplementary Fig. S6b). Consistently, serum and hepatic TG and TC levels were also significantly reduced after LFW273 and resmetirom treatment (Fig. 7d; Supplementary Fig. S6c). The improvement in HSC activation and collagen deposition was indicated by reduced positive staining with Masson, Sirius red, and immunohistochemical staining for α-SMA and COL1A1 (Fig. 7c and e); accordingly, the grade of NAS was decreased (Supplementary Fig. S6d). Moreover, the protein levels of α-SMA and COL1A1 were decreased in the livers of LFW273- and resmetirom-treated mice, as detected by immunoblotting (Fig. 7f). We also observed a reduction in hepatic SNAI1 expression in

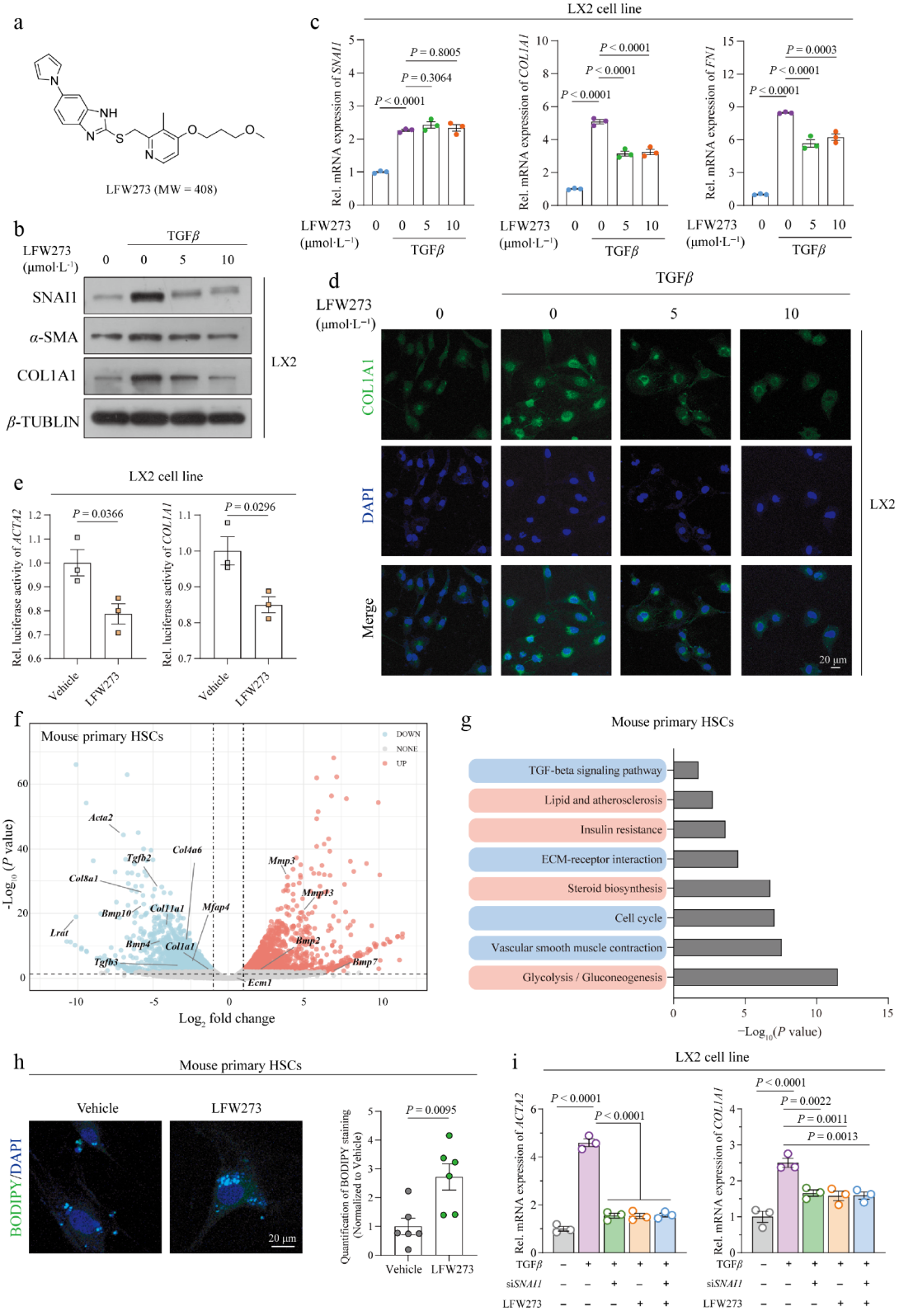


Fig. 4 LFW273, a SNAI1-specific inhibitor, suppressed the activation of HSCs. (a) The construction and molecular weight of LFW273. LX2 cells were treated with 10 μmol·L^{-1} TGF-*β* for 12 h, followed by LFW273 at 5 or 10 μmol·L^{-1} for 48 h. (b) Protein levels of SNAI1, *α*-SMA (*ACTA2*) and COL1A1. (c) mRNA expression of *SNAI1*, *COL1A1*, and *FN1*. (d) Immunofluorescent staining with anti-COL1A1 antibody. Scale bar: 20 μm. (e) Transcriptional activity of *ACTA2* and *COL1A1* in LX2 cells treated with TGF-*β* and 5 μmol·L^{-1} LFW273. Primary HSCs activated by FBS for 7 d *in vitro* and treated with vehicle or LFW273 for 48 h. (f) Volcano plot of differentially expressed pro-fibrotic genes ($\log_2$FC > 1 and *P* value < 0.05). (g) Kyoto Encyclopedia of Genes and Genomes (KEGG) pathway enrichment analysis. (h) Representative images of BODIPY staining (left) and quantification (right). Scale bar: 20 μm. (i) LX2 cells were transfected with si*SNAI1* or siScramble and were treated with TGF-*β* (10 μmol·L^{-1}) for 12 h, followed by 10 μmol·L^{-1} LFW273 for 48 h. mRNA level of *ACTA2* and *COL1A1*. Data are presented as mean ± SEM. *P* < 0.05 indicates a significant difference. All data were analyzed by two-tailed Student's t-test or one-way ANOVA with Dunnett's multiple comparisons test.

https://doi.org/10.48130/targetome-0026-0060

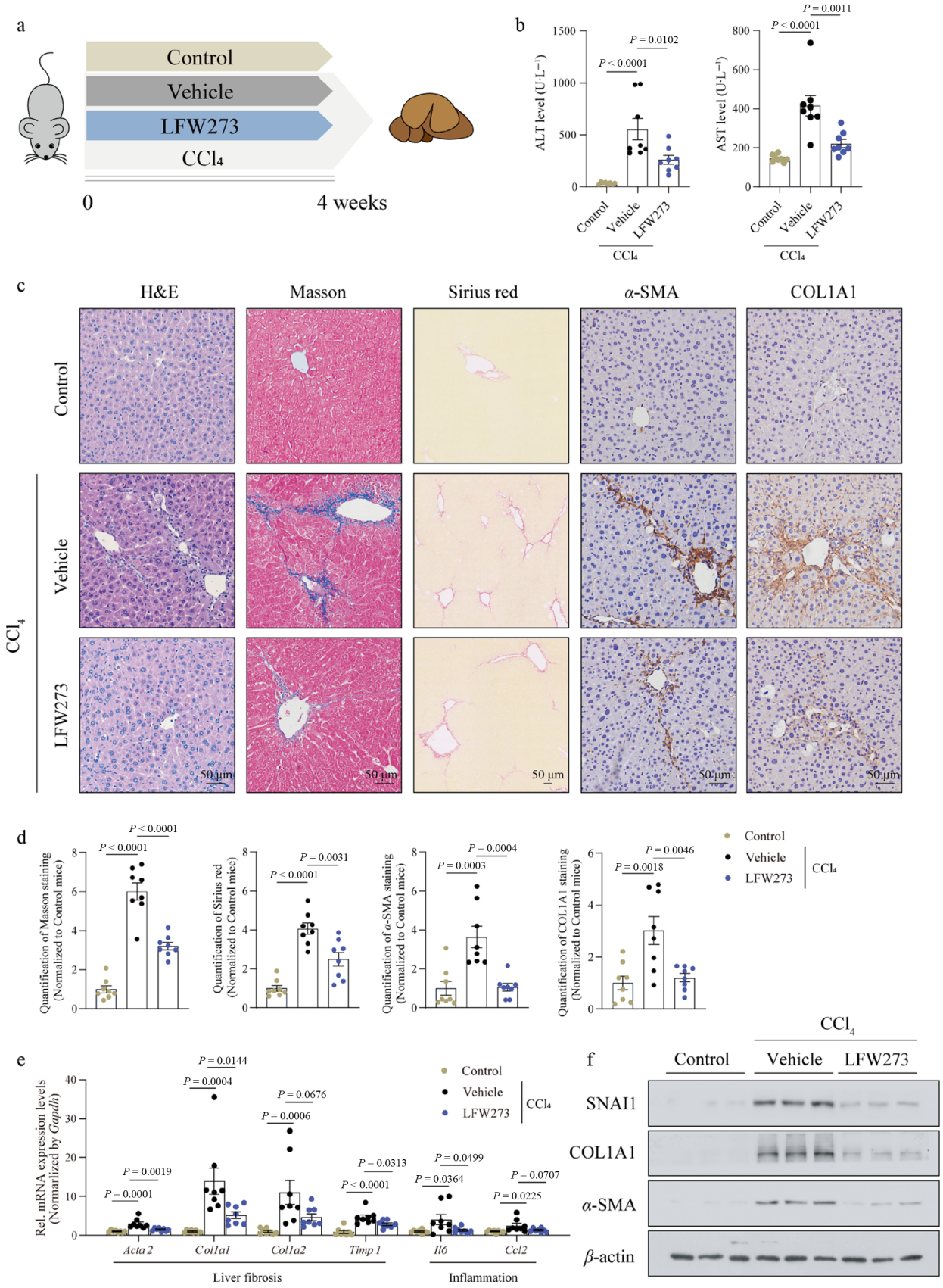


Fig. 5 Pharmacological inhibition of SNAI1 by LFW273 prevented CCl_4-induced liver fibrosis in mice. Mice were injected with CCl_4 and administered LFW273 for 4 weeks (n = 8 per group). (a) Schematic of the mouse model. (b) Serum ALT and AST. (c) Representative images of H&E, Masson, Sirius red, α-SMA and COL1A1 immunohistochemistry staining. Scale bar: 50 μm. (d) Quantification of positive staining areas in (c). (e) Gene expression of *Acta2*, *Col1a1*, *Col1a2*, *Timp1*, *Il6*, and *Ccl2*. (f) Protein levels of SNAI1, COL1A1, and α-SMA in liver tissues. Data are presented as mean ± SEM. $p < 0.05$ indicates a significant difference. All data were analyzed by one-way ANOVA with Dunnett's multiple comparisons test.

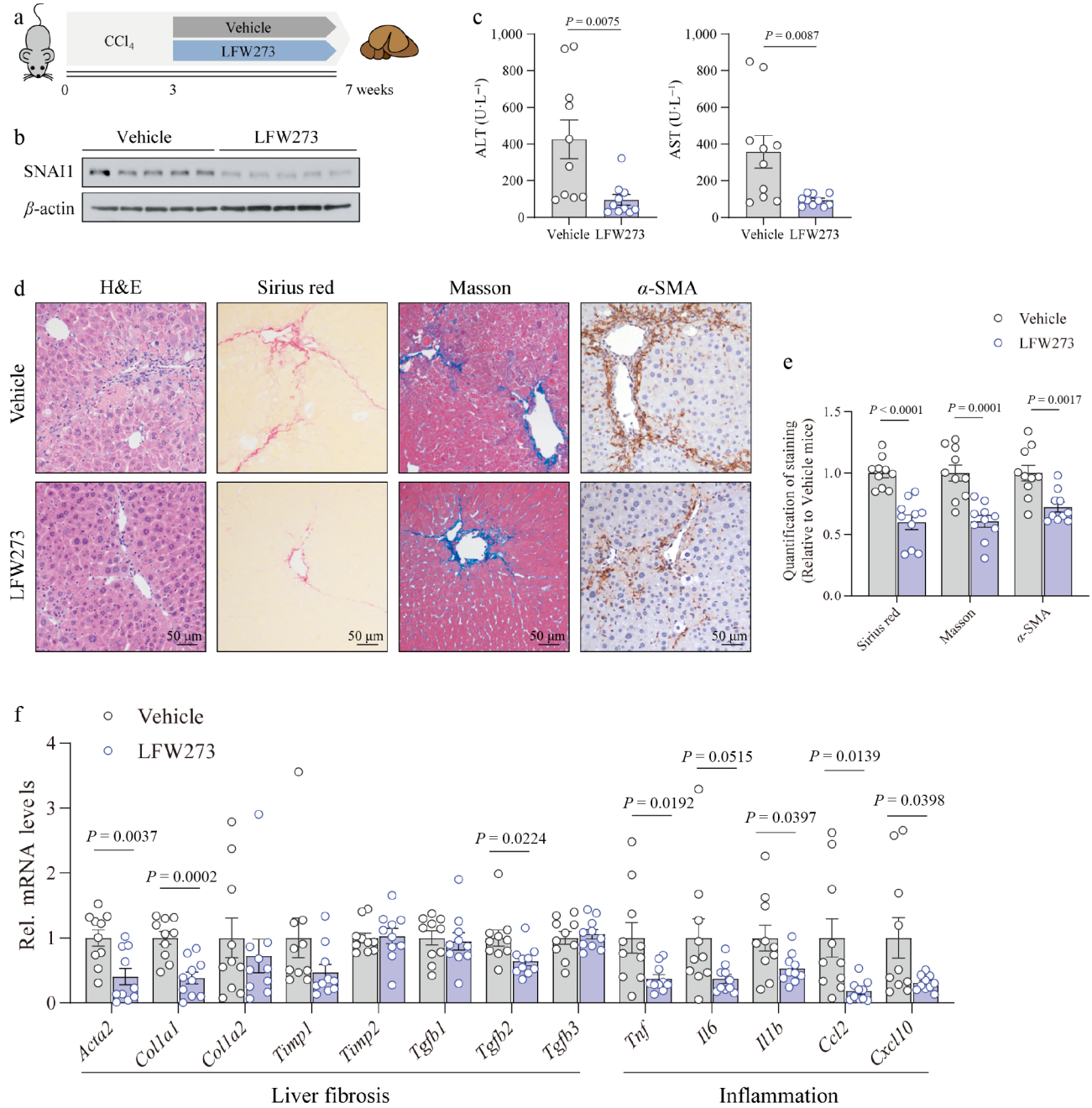


Fig. 6 LFW273 alleviated the development of liver fibrosis in mice pre-treated with CCl_4. Mice were injected with CCl_4 for 3 weeks, followed by gavage administration of LFW273 at a dose of 100 mg·kg^{-1} for an additional 4 weeks (n = 10 per group). (a) Schematic of the mouse model. (b) Immunoblotting of SNAI1. (c) ALT and AST levels in serum. (d) Representative images of H&E, Sirius red, Masson, and α-SMA staining. Scale bar: 50 μm. (e) Quantification of positive staining on liver sections. (f) Gene expressions of *Acta2*, *Col1a1*, *Col1a2*, *Timp1*, *Timp2*, *Tgfb1*, *Tgfb2*, *Tgfb3,* and pro-inflammatory genes including *Tnf*, *Il6*, *Il1b*, *Ccl2,* and *Cxcl10* in liver tissues. Data are presented as mean ± SEM. $p < 0.05$ indicates a significant difference. All data were analyzed by a two-tailed Student's t-test.

resmetirom-treated mice. This decrease is unlikely to be a direct effect of resmetirom on HSCs, as resmetirom did not affect SNAI1 expression in TGF-β-activated LX2 cells (Supplementary Fig. S6e). Furthermore, fibrosis-related genes (*Acta2*, *Col1a1*, *Col1a2*, *Timp2*, *Tgfb2*, and *Tgfb3*) and inflammatory cytokines and chemokine genes (*Tnf*, *Il1b*, *Il6*, *Ccl2*, and *Ccl5*) were downregulated in mice subjected to pharmacological therapy (Fig. 7g and h; Supplementary Fig. S6f).

Collectively, all our results demonstrated that LFW273, a small-molecule inhibitor of SNAI1, is capable of ameliorating MASH-induced liver fibrosis, indicating the potential clinical application of this lead compound LFW273 in MASH treatment.

Discussion

Liver fibrosis is a complication of many chronic liver diseases and remains a major therapeutic challenge[1,2]. Although considerable progress has been made in identifying anti-fibrotic targets and developing candidate drugs, few have been approved for clinical use[40–42]. In this study, we demonstrated that SNAI1, a zinc-finger transcription factor mainly expressed in HSCs, was increased upon HSC activation in patients with liver fibrosis. We further revealed that SNAI1 promoted liver fibrosis progression by directly binding to the promoters of the HSC activation marker genes *ACTA2* and

https://doi.org/10.48130/targetome-0026-0060

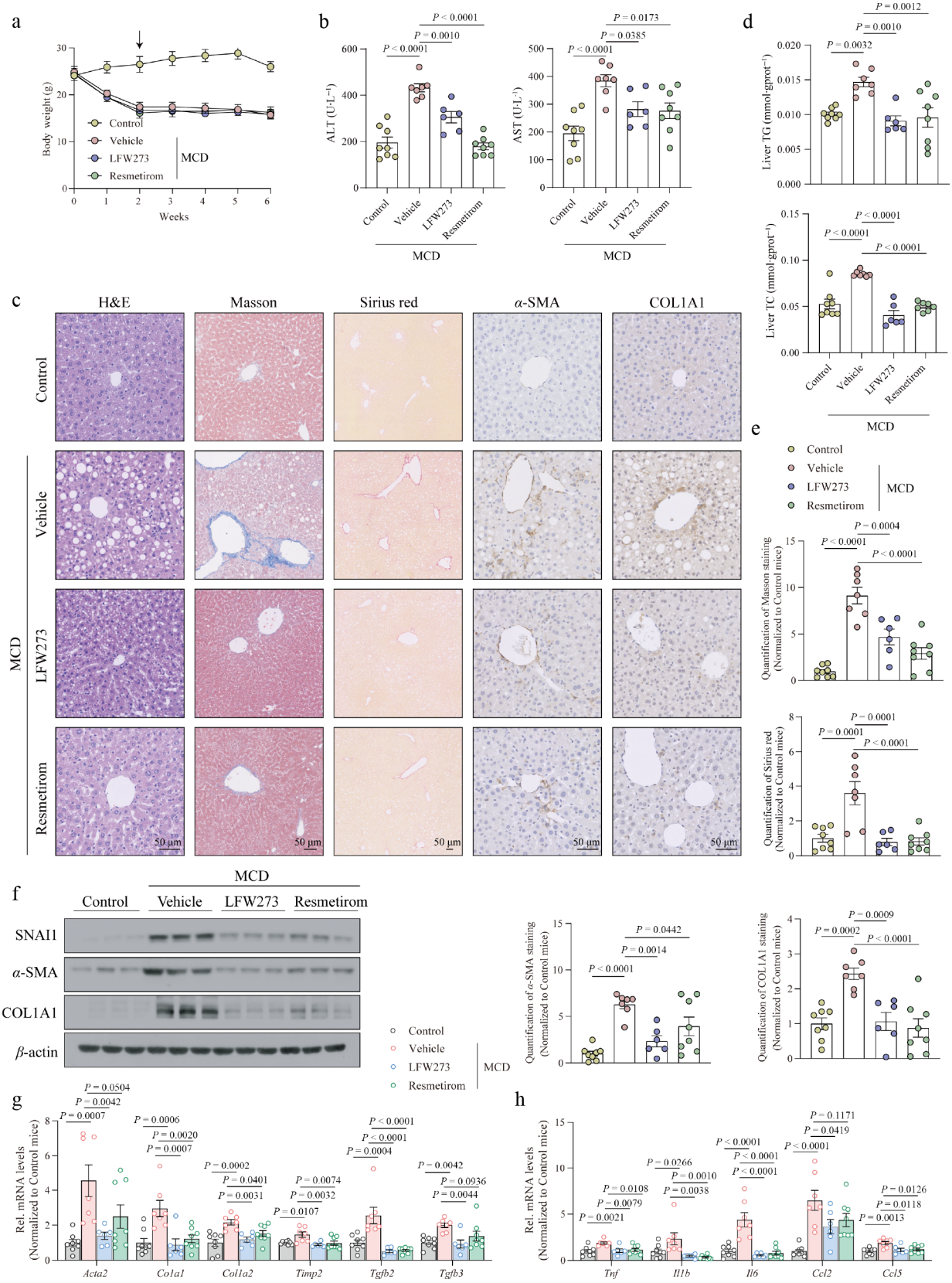


Fig. 7 MASH-accompanied liver fibrosis was abolished by LFW273 treatment. Mice were fed an MCD diet for 2 weeks, followed by LFW273 and resmetirom administration for an additional 4 weeks (n = 8 for Control; n = 7 for vehicle; n = 6 for LFW273; n = 8 for resmetirom). (a) Body weight. (b) Serum ALT and AST. (c) Representative image of H&E, Masson, Sirius red, and immunohistochemistry staining with anti-α-SMA and anti-COL1A1 antibodies. Scale bar: 50 μm. (d) Hepatic levels of TG and TC. (e) Quantification of positive areas in (c). (f) Protein levels of SNAI1, α-SMA, and COL1A1 in liver tissues. (g) Expression of genes encoding HSC activation and collagen production. (h) Expression of genes related to liver inflammation. Data are presented as mean ± SEM. P < 0.05 indicates a significant difference. All data were analyzed by ordinary one-way ANOVA with Dunnett's multiple comparisons test.

COL1A1, and enhanced histone acetylation at H3K4, H3K14, and H3K18 upon HSC activation. Moreover, genetic and pharmacological inhibition of SNAI1 protected mice from CCl_4- or MASH-induced liver fibrosis, supporting the idea that SNAI1 might be a promising therapeutic target for anti-fibrotic therapy.

Most studies on SNAI1 have concentrated on its functions in EMT during tumor progression[9,43,44]. Its pathophysiological roles in non-tumor tissues such as atherosclerosis, renal fibrosis, and muscle regeneration have been recently reported[11,30,45]. Regarding the roles of SNAI1 in liver fibrosis, unlike earlier studies that focused on SNAI1 in hepatocytes[15], our findings demonstrated that the expression of SNAI1 was substantially higher in HSCs than in other cell types, including hepatocytes, KCs, and LSECs. Despite these existing differences, our findings are more consistent with the pathogenesis of liver fibrosis, in which HSCs become activated and transform into myofibroblasts, promoting the production of collagen and ECM. scRNA-sequencing analysis, β-gal/α-SMA co-staining, and immunoblotting of different cells isolated from fibrotic mouse livers confirmed this result. These complementary approaches avoided the false positives and misinterpretation caused by the low specificity of the anti-SNAI1 antibody, providing solid evidence for SNAI1 function in liver fibrosis.

A recent study reported that the hepatic *Snai1* and *Snai2* promoted liver regeneration and suppressed liver fibrosis[16], seemingly contradicting our findings. However, that study focused on different cell types from ours, and HSCs play much more direct roles in liver fibrosis. Moreover, their hepatocyte-specific ablation of *Snai1* and *Snai2* limited the ability to investigate the function of SNAI1 in liver fibrosis. In contrast, using HSC-specific *Snai1* deletion mice, our study demonstrates its pro-fibrotic role more directly.

Liver fibrosis is driven by complex crosstalk between HSCs and surrounding cells[2,46,47]. Activated HSCs secrete cytokines, further influencing immune cells and hepatocytes[48,49]. Consistently, we observed reduced liver inflammation and a slight increase in hepatocyte proliferation in HSC-specific *Snai1*-deficient mice. Although not all the inflammation-related genes were downregulated, these phenotypes may reflect the crosstalk between HSCs and other cell types.

In the present study, we demonstrated that LFW273 acts as a specific SNAI1 inhibitor, which decreases the stability of SNAI1[30]. Oral administration of LFW273 protected mice from CCl_4 or MASH-induced liver fibrosis, as evidenced by reduced HSC activation, collagen deposition, and inflammation. Although we demonstrated that LFW273 protects HSCs from activation by inhibiting SNAI1 (Fig. 4i), whether its anti-fibrotic efficacy relies solely on SNAI1 in HSCs requires further exploration. Notably, inflammation and endothelial-to-mesenchymal transition (EndMT) of LSECs contribute to liver fibrosis[2,50,51], and SNAI1 has been implicated in both inflammatory chemokine production and EndMT[30,52,53]. LFW273 treatment also suppressed the inflammatory genes in RAW 264.7 mouse macrophages (Supplementary Fig. S7). Therefore, pharmacological inhibition of SNAI1 by LFW273 may improve liver fibrosis not only by acting directly on HSCs, but also potentially by modulating KCs and LSECs.

A characteristic feature of quiescent HSCs is the abundance of lipid droplets. The loss of lipid droplets acts as a hallmark of HSC activation and is necessary for this critical event. Therefore, maintaining lipid droplet integrity may represent a valid strategy to reduce HSC activation[33]. In this study, we observed that steroid biosynthesis and insulin resistance pathways were significantly activated in primary HSCs after LFW273 treatment, which was associated with reduced HSC activation. Moreover, ChIP assay confirmed the binding of SNAI1 to the *PPARG* promoter, suggesting that LFW273 promotes maintenance of the lipid-rich quiescent HSCs by relieving *PPARG* repression. Given that SNAI1 is barely expressed in hepatocytes, the improvement in hepatic steatosis in MASH mice is unlikely to be mediated by a direct SNAI1-*PPARG*-dependent mechanism. Instead, these effects may result from indirect crosstalk between HSCs, immune cells (such as KCs), and hepatocytes, as inflammation is known to promote hepatic lipid accumulation[54,55]. Nevertheless, the mechanism by which SNAI1 inhibitor affects hepatic steatosis remains to be investigated to further elucidate its potential for anti-MASH therapy.

Evidence shows that the prevalence of MASH-induced fibrosis has progressively risen[39], with only two drugs, resmetirom and semaglutide, approved by the FDA for MASH therapy[5–7]. In this study, we chose resmetirom as the positive control. Although resmetirom treatment reduced SNAI1 levels in fibrotic mouse livers (Fig. 7e), it did not suppress the expression of SNAI1 in HSCs (Supplementary Fig. S6e), which is consistent with resmetirom improving liver fibrosis by targeting THRb in hepatocytes and affecting HSCs indirectly *via* intercellular crosstalk. In contrast, LFW273 treatment acts more directly on HSCs and thereby abolishes HSC activation and collagen accumulation.

However, it should be noted that MCD-induced MASH, which causes decreased body weight and lacks insulin resistance, does not recapitulate the metabolic features of clinical MASH, despite its wide use for rapid fibrosis establishment[56]. Long-term MASH models, such as those induced by GAN diet or CDAHFD, are more suitable for phenocopying clinical MASH. Nevertheless, the MCD-induced MASH-associated fibrosis model remains a valuable tool for the preliminary evaluation of anti-fibrotic drugs. Regarding LFW273, despite the acceptable oral bioavailability (~50%), its relatively high effective dose and short plasma $t_{1/2}$ (~2.85 h) suggest the need for further structural modification and optimization to improve its pharmacokinetic properties. Once optimized candidates are identified, their efficacy and safety will be systematically evaluated in long-term MASH models to further validate their anti-fibrotic potential.

Conclusions

Collectively, our study delineated the pro-fibrotic function of SNAI1 in HSCs, and SNAI1 increases the transcription of *ACTA2* and *COL1A1 via* epigenetic regulation of their promoters to accelerate liver fibrosis. More importantly, genetic inhibition of *Snai1* and pharmacological inhibition by LFW273 effectively protected mice from CCl_4-induced liver fibrosis. LFW273 treatment also demonstrated remarkable effects in MCD-induced fibrosis, comparable to those of resmetirom treatment. These findings indicate that SNAI1 might be a promising drug target for liver fibrosis therapy, and that LFW273 could serve as a potential lead compound for further optimization.

Ethical statements

All procedures were reviewed and pre-approved by the Institutional Animal Care and Use Committee of China Pharmaceutical University (YSL-202504067, approval date: 2025−4−14). The research followed the 'Replacement, Reduction, and Refinement' principles to minimize harm to animals. This article provides details on the housing conditions, care, and pain management for the animals, ensuring that the impact on the animals is minimized during the experiment.

Author contributions

The authors confirm their contributions to the paper as follows: study conception and design: Wu ZQ, Fu R, Liu J; data collection: Pan C, Zhang XZ, Xu XW; analysis and interpretation of results: Pan C, Zeng ZL, Weiss SJ; draft manuscript preparation: Pan C, Wu ZQ, Fu R. All authors reviewed the results and approved the final version of the manuscript.

Data availability

RNA-seq data have been deposited in GEO and are publicly available under accession number GSE329196. All data reported in this paper are available from the corresponding author upon reasonable request.

Acknowledgments

This work was supported by the Jiangsu Provincial Natural Science Fund (BK20230042 and BK20241595), the National Key Research and Development Program of China (2023YFA1801900), the National Ten Thousand Talents Program for Young Top-notch Talents, the National Natural Science Foundation of China (82125036, 82273964, 82404693, and 82675055), the Jiangsu Provincial Outstanding Postdoctoral Program, the China Postdoctoral Science Foundation (2025M773558), and the Specialized Research Funds from the State Key Laboratory of Natural Medicines, China Pharmaceutical University.

Conflict of interest

The authors have no conflict of interest to declare.

Supplementary information accompanies this paper online at: https://doi.org/10.48130/targetome-0026-0060.

Dates

Received 20 April 2026; Revised 7 September 2026; Accepted 14 September 2026; Published online 11 November 2026

References

[1] Kisseleva T, Brenner D. 2021. Molecular and cellular mechanisms of liver fibrosis and its regression. *Nature Reviews Gastroenterology & Hepatology* 18:151−166

[2] Hammerich L, Tacke F. 2023. Hepatic inflammatory responses in liver fibrosis. *Nature Reviews Gastroenterology & Hepatology* 20:633−646

[3] Parola M, Pinzani M. 2019. Liver fibrosis: pathophysiology, pathogenetic targets and clinical issues. *Molecular Aspects of Medicine* 65:37−55

[4] Friedman SL, Pinzani M. 2022. Hepatic fibrosis 2022: unmet needs and a blueprint for the future. *Hepatology* 75:473−488

[5] Keam SJ. 2024. Resmetirom: first approval. *Drugs* 84:729−735

[6] Brisnovali NF, Haney C, Goedeke L. 2024. Rezdiffra™ (resmetirom): a THR-β agonist for non-alcoholic steatohepatitis. *Trends in Pharmacological Sciences* 45:1081−1082

[7] Bansal MB, Patton H, Morgan TR, Carr RM, Dranoff JA, et al. 2026. Semaglutide therapy for metabolic dysfunction – associated steatohepatitis: November 2025 updates to AASLD practice guidance. *Hepatology* 83:1326−1340

[8] Noureddin M, Kowdley KV, Odrljin T, Bain G, Zhao J, et al. 2026. Efimosfermin alfa (BOS-580) once per month in people with metabolic dysfunction-associated steatohepatitis with F2 or F3 fibrosis: results from a 24-week, randomised, double-blind, placebo-controlled, phase 2 trial. *The Lancet* 407:794−804

[9] Ni T, Li XY, Lu N, An T, Liu ZP, et al. 2016. Snail1-dependent p53 repression regulates expansion and activity of tumour-initiating cells in breast cancer. *Nature Cell Biology* 18:1221−1232

[10] Wu ZQ, Rowe RG, Lim KC, Lin Y, Willis A, et al. 2014. A Snail1/Notch1 signalling axis controls embryonic vascular development. *Nature Communications* 5:3998

[11] Grande MT, Sánchez-Laorden B, López-Blau C, De Frutos CA, Boutet A, et al. 2015. Snail1-induced partial epithelial-to-mesenchymal transition drives renal fibrosis in mice and can be targeted to reverse established disease. *Nature Medicine* 21:989−997

[12] Manetti M, Romano E, Rosa I, Guiducci S, Bellando-Randone S, et al. 2017. Endothelial-to-mesenchymal transition contributes to endothelial dysfunction and dermal fibrosis in systemic sclerosis. *Annals of the Rheumatic Diseases* 76:924−934

[13] Jayachandran A, Königshoff M, Yu H, Rupniewska E, Hecker M, et al. 2009. SNAI transcription factors mediate epithelial-mesenchymal transition in lung fibrosis. *Thorax* 64:1053−1061

[14] Chu AS, Diaz R, Hui JJ, Yanger K, Zong Y, et al. 2011. Lineage tracing demonstrates no evidence of cholangiocyte epithelial-to-mesenchymal transition in murine models of hepatic fibrosis. *Hepatology* 53:1685−1695

[15] Rowe RG, Lin Y, Shimizu-Hirota R, Hanada S, Neilson EG, et al. 2011. Hepatocyte-derived Snail1 propagates liver fibrosis progression. *Molecular and Cellular Biology* 31:2392−2403

[16] Wang P, Kang Q, Wu WS, Rui L. 2024. Hepatic *Snai1* and Snai2 promote liver regeneration and suppress liver fibrosis in mice. *Cell Reports* 43:113875

[17] Bao L, Chu Y, Kang H. 2023. SNAI1-activated long non-coding RNA LINC01711 promotes hepatic fibrosis cell proliferation and migration by regulating XYLT1. *Genomics* 115:110597

[18] Tan S, Lu Y, Xu M, Huang X, Liu H, et al. 2019. β-Arrestin1 enhances liver fibrosis through autophagy - mediated Snail signaling. *The FASEB Journal* 33:2000−2016

[19] Sugimoto A, Saito Y, Wang G, Sun Q, Yin C, et al. 2025. Hepatic stellate cells control liver zonation, size and functions *via* R-spondin 3. *Nature* 640:752−761

[20] Trépo E, Goossens N, Fujiwara N, Song WM, Colaprico A, et al. 2018. Combination of gene expression signature and model for end-stage liver disease score predicts survival of patients with severe alcoholic hepatitis. *Gastroenterology* 154:965−975

[21] Jeong BK, Choi WI, Choi W, Moon J, Lee WH, et al. 2024. A male mouse model for metabolic dysfunction-associated steatotic liver disease and hepatocellular carcinoma. *Nature Communications* 15:6506

[22] Steixner-Kumar AA, Santacruz D, Geiger T, Rust W, Böttner D, et al. 2025. Single-cell landscape of peripheral immune cells in MASLD/MASH. *Hepatology Communications* 9:e0643

[23] Uchinami H, Seki E, Brenner DA, D'Armiento J. 2006. Loss of MMP 13 attenuates murine hepatic injury and fibrosis during cholestasis. *Hepatology* 44:420−429

[24] Wang L, Mazagova M, Pan C, Yang S, Brandl K, et al. 2019. YIPF6 controls sorting of FGF21 into COPII vesicles and promotes obesity. *Proceedings of the National Academy of Sciences of the United States of America* 116:15184−15193

[25] Li ZW, Ruan B, Yang PJ, Liu JJ, Song P, et al. 2023. Oit3, a promising hallmark gene for targeting liver sinusoidal endothelial cells. *Signal Transduction and Targeted Therapy* 8:344

[26] Mederacke I, Dapito DH, Affò S, Uchinami H, Schwabe RF. 2015. High-yield and high-purity isolation of hepatic stellate cells from normal and fibrotic mouse livers. *Nature Protocols* 10:305−315

[27] Pan C, Liu J, Gao Y, Yang M, Hu H, et al. 2023. Hepatocyte CHRNA4 mediates the MASH-promotive effects of immune cell-produced acetylcholine and smoking exposure in mice and humans. *Cell Metabolism* 35:2231−2249. e7

[28] Gao YS, Qian MY, Wei QQ, Duan XB, Wang SL, et al. 2020. WZ66, a novel acetyl-CoA carboxylase inhibitor, alleviates nonalcoholic steatohepatitis (NASH) in mice. *Acta Pharmacologica Sinica* 41:336−347

[29] Ren B, Li Y, Di L, Cheng R, Liu L, et al. 2024. A naturally derived small molecule compound suppresses tumor growth and metastasis in mice

by relieving p53-dependent repression of CDK2/Rb signaling and the Snail-driven EMT. *Chinese Journal of Natural Medicines* 22:112−126
[30] Ren BX, Zeng ZL, Deng L, Hu JM, Chen MZ, et al. 2025. Genetic and pharmacological targeting of Snail inhibits atherosclerosis by relieving intraplaque endothelium dysfunction and associated inflammation. *Acta Pharmacologica Sinica* 46:2196−2212
[31] Geng F, Zhong Y, Su H, Lefai E, Magaki S, et al. 2023. SREBP-1 upregulates lipophagy to maintain cholesterol homeostasis in brain tumor cells. *Cell Reports* 42:112790
[32] Tao J, Wu Z, Liang Y, Wang J, Tang M, et al. 2025. Lhx2 specifically expressed in HSCs promotes liver regeneration and inhibits liver fibrosis. *Hepatology* 82:683−701
[33] Schwabe RF, Brenner DA. 2025. Hepatic stellate cells: balancing homeostasis, hepatoprotection and fibrogenesis in health and disease. *Nature Reviews Gastroenterology & Hepatology* 22:481−499
[34] Yang W, He H, Wang T, Su N, Zhang F, et al. 2021. Single-cell transcriptomic analysis reveals a hepatic stellate cell–activation roadmap and myofibroblast origin during liver fibrosis in mice. *Hepatology* 74:2774−2790
[35] Cano A, Pérez-Moreno MA, Rodrigo I, Locascio A, Blanco MJ, et al. 2000. The transcription factor Snail controls epithelial-mesenchymal transitions by repressing E-cadherin expression. *Nature Cell Biology* 2:76−83
[36] Singh D, Deshmukh RK, Das A. 2021. SNAI1-mediated transcriptional regulation of epithelial-to-mesenchymal transition genes in breast cancer stem cells. *Cellular Signalling* 87:110151
[37] Hazra S, Xiong S, Wang J, Rippe RA, Krishna V, et al. 2004. Peroxisome proliferator-activated receptor γ induces a phenotypic switch from activated to quiescent hepatic stellate cells. *Journal of Biological Chemistry* 279:11392−11401
[38] Sharvit E, Abramovitch S, Reif S, Bruck R. 2013. Amplified inhibition of stellate cell activation pathways by PPAR-γ, RAR and RXR agonists. *PLoS One* 8:e76541
[39] Man S, Deng Y, Ma Y, Fu J, Bao H, et al. 2023. Prevalence of liver steatosis and fibrosis in the general population and various high-risk populations: a nationwide study with 5. *7 million adults in China. Gastroenterology* 165:1025−1040
[40] Zhao M, Wang L, Wang M, Zhou S, Lu Y, et al. 2022. Targeting fibrosis: mechanisms and clinical trials. *Signal Transduction and Targeted Therapy* 7:206
[41] Parola M, Pinzani M. 2024. Liver fibrosis in NAFLD/NASH: from pathophysiology towards diagnostic and therapeutic strategies. *Molecular Aspects of Medicine* 95:101231
[42] Kumar V, Xin X, Ma J, Tan C, Osna N, et al. 2021. Therapeutic targets, novel drugs, and delivery systems for diabetes associated NAFLD and liver fibrosis. *Advanced Drug Delivery Reviews* 176:113888
[43] Bao Z, Zeng W, Zhang D, Wang L, Deng X, et al. 2022. SNAIL induces EMT and lung metastasis of tumours secreting CXCL2 to promote the invasion of M2-type immunosuppressed macrophages in colorectal cancer. *International Journal of Biological Sciences* 18:2867−2881
[44] Carmichael CL, Wang J, Nguyen T, Kolawole O, Benyoucef A, et al. 2020. The EMT modulator SNAI1 contributes to AML pathogenesis *via* its interaction with LSD1. *Blood* 136:957−973
[45] Elia I, Realini G, Di Mauro V, Borghi S, Bottoni L, et al. 2022. SNAI1 is upregulated during muscle regeneration and represses FGF21 and ATF3 expression by directly binding their promoters. *The FASEB Journal* 36:e22401
[46] Yang F, Li H, Li Y, Hao Y, Wang C, et al. 2021. Crosstalk between hepatic stellate cells and surrounding cells in hepatic fibrosis. *International Immunopharmacology* 99:108051
[47] Lan R, Lin J, Chen S, Lu Z, Gong Y, et al. 2025. Communication initiated by hepatocytes: the driver of HSC activation and liver fibrosis. *Hepatology Communications* 9:e0753
[48] Gupta G, Khadem F, Uzonna JE. 2019. Role of hepatic stellate cell (HSC)-derived cytokines in hepatic inflammation and immunity. *Cytokine* 124:154542
[49] Qian H, Deng X, Huang ZW, Wei J, Ding CH, et al. 2015. An HNF1α-regulated feedback circuit modulates hepatic fibrogenesis *via* the crosstalk between hepatocytes and hepatic stellate cells. *Cell Research* 25:930−945
[50] Tsuchida T, Friedman SL. 2017. Mechanisms of hepatic stellate cell activation. *Nature Reviews Gastroenterology & Hepatology* 14:397−411
[51] Felli E, Nulan Y, Ortega-Ribera M, Fernández-Iglesias A, Gracia-Sancho J. 2026. The role of liver sinusoidal endothelial cells in liver diseases: key players in health and pathology. *Journal of Hepatology* 84:655−672
[52] Zhou Y, Zhao D, Ma Q, Xu J, Cai Y, et al. 2025. Endothelial adenosine receptor 2A loss alleviates diabetic vascular calcification by blocking CREB1-SNAI1-driven EndMT. *Pharmacological Research* 221:107981
[53] Xu X, Tan X, Tampe B, Sanchez E, Zeisberg M, et al. 2015. Snail is a direct target of hypoxia-inducible factor 1α (HIF1α) in hypoxia-induced endothelial to mesenchymal transition of human coronary endothelial cells. *Journal of Biological Chemistry* 290:16653−16664
[54] Ma KL, Ruan XZ, Powis SH, Chen Y, Moorhead JF, et al. 2008. Inflammatory stress exacerbates lipid accumulation in hepatic cells and fatty livers of apolipoprotein E knockout mice. *Hepatology* 48:770−781
[55] Cai Y, Li H, Liu M, Pei Y, Zheng J, et al. 2018. Disruption of adenosine 2A receptor exacerbates NAFLD through increasing inflammatory responses and SREBP1c activity. *Hepatology* 68:48−61
[56] Gallage S, Avila JEB, Ramadori P, Focaccia E, Rahbari M, et al. 2022. A researcher's guide to preclinical mouse NASH models. *Nature Metabolism* 4:1632−1649

Copyright: © 2026 by the author(s). Published by Maximum Academic Press on behalf of China Pharmaceutical University. This article is an open access article distributed under Creative Commons Attribution License (CC BY 4.0), visit https://creativecommons.org/licenses/by/4.0/.